ICAS 2020 SHANG HAI
International Council of the Aeronautical Sciences
32nd Congress of the International Council of the Aeronautical Sciences
September 6-10, 2021
Pudong Shangri-La, Shanghai, China

Integrated Aerodynamic Design of Propeller Position and Wing Shape at a Low Reynolds Number

YANG Wei[1,2], YU Lei[2,*], WU Wenhua[2]& FAN Zhaolin[1,2]

[1]College of Aerospace Science and Engineering, National University of Defense Technology, Changsha 410073, China
[2]China Aerodynamics Research and Development Center, Mianyang 621000, China

Abstract

The slipstream of near space multi-propeller aircraft has great influence on the flow around the wing. A method of integrated aerodynamic optimization design of propeller position and wing shape at a low Reynolds number is presented to improve the integrated aerodynamic performance of the leading-edge propeller configuration at cruise condition. First, computational fluid dynamics (CFD) method was adopted to calculate and analyze the aerodynamic forces on the basis of three dimensional Reynolds-averaged Navier-Stokes (RANS) solver employing k-ω SST turbulence model coupled with γ-$Re_{\theta t}$ transition prediction mode. The equivalent actuator disk model was employed to simulate the slipstream of real propeller in a quick and efficient way. Second, free-form deformation (FFD) technology was used for the parameterization of the wing. A grid deformation method based on radial basis function (RBF) interpolation was embedded in optimization for high-speed regeneration of grids around a new wing. Grids of the propeller in a new position were obtained by translation transformation. The computational grids of the integrated leading-edge propeller/wing configuration were generated by combining the grids of the propeller with those of the wing by overset method. Finally, an integrated aerodynamic optimization design system was established based on quantum-behaved particle swarm optimization (QPSO) algorithm and aforementioned methods. The system was applied to the integrated aerodynamic design of the propeller position and the wing shape of a propeller/wing configuration at a low Reynolds number, taking into account the propeller slipstream effect. Results indicated that the lift-to-drag ratio of the optimized configuration was greatly improved by 65.9%, compared to the initial one. This could be conducive to heavier mission load and lower energy consumption of the near space multi-propeller aircraft.

Keywords: aerodynamic design, propeller position, wing shape, low Reynolds number

1. Introduction

Near space has become a hot area of aviation engineering research all over the world, due to its unique resource advantages and strategic value. High altitude and long endurance (HALE) solar powered unmanned aerial vehicles (UAVs), which convert solar energy into electricity to drive propellers, are theoretically capable of flying literally "forever" at high altitudes or in close space [1]. Driven by advanced aviation technology and strong demand, HALE solar UAVs show very broad military and civil prospects [2,3].

The solar UAVs cruise at low density and Reynolds number condition of upper stratosphere, therefore, experience a quite low aerodynamic efficiency, as well as propulsion efficiency. The payload of the UAVs is relatively limited, because the lift coefficient is not high, which greatly limits the use of solar drones to a certain extent. Traditional design of solar powered UAVs employs very large wing area and aspect ratio to improve the aerodynamic characteristics, and multiple leading-edge propellers to increase propulsion performance. In order to promote endurance and carry more payloads, lots of studies were attempt to enhance the overall aerodynamic performance of the vehicle by improve the aerodynamic characteristics of the airfoil and the wing. Some scholars focus on the studies of airfoil design and three-dimensional wing design at the condition of pure inflow, others realized that the slipstream of multiple propellers had a great widespread impact to

the wing and took slipstream effect of fixed propellers into account [4,5].

In recent years, distributed electric propulsion (DEP) technology has been applied more and more widely in the aviation field [6,7]. DEP technology emphasizes the use of multiple small electric propellers instead of a few large propellers. One of the important reasons is that the slipstreams of the distributed multiple propellers can cover most of the wing along the span, so that the aircrafts can make full use of slipstream lift to greatly improve the aerodynamic performance of the wings, so as to meet the requirements of lifting load and long endurance flight [8]. The DEP technology has been soon applied to the research of solar powered UAV. Wang K [9] and Wang H [10] respectively studied the aerodynamic influence of distributed propeller slip flow on solar-powered unmanned aerial vehicle. They found that propellers slipstreams would increase the lift and drag of the wing, decrease the lift-drag ratio, and also inhibit flow separation. Wang K [5] also carried out a study on the coupling aerodynamic design of a multiple propellers/wing configuration. Parameters were designed firstly, such as the number of propellers, diameter, pitch between the propeller and the wing, and then the shape of the wing was optimized to improve the aerodynamic performance of the configuration.

Compared with the large propeller power system, the influence of multiple propellers on the boundary layer the downstream wing is much greater. This means propeller position, especially, the height, has a dominant influence on the slipstream region and the downstream flow around the wing. Therefore, propeller position is a significant and non-negligible factor in aerodynamic design. Unawareness of either the existence or the location of the propellers in design will lead to the deviation of overall aerodynamic performance and endurance of the UAVs. However, considering the influence of the distributed propeller slipstream on the aerodynamic performance of the wing, the coupling optimization design is rarely studied of the distributed propeller installation position and the aerodynamic profile of the wing.

In this thesis, a method of integrated aerodynamic optimization design of propeller position and wing shape is presented to improve the integrated aerodynamic performance of the leading-edge propeller configuration in cruise condition at a low Reynolds number. CFD method on the basis of three dimensional Reynolds-averaged Navier-Stokes solver was used to calculate and analyze the aerodynamic forces. The equivalent actuator disk model was employed to simulate the slipstream of real propeller in a quick and efficient way. FFD technology was used for parameterization of the wing, which was a mature method in the aspect of aircraft shape parameterization and could accurately describe the locality of surface deformation. A grid deformation method based on radial basis function (RBF) interpolation was embedded in optimization for fast and robust regeneration of grids around a new wing. Grids of the propeller in a new position were obtained by translation transformation. The grids of the propeller were then combined with those of the wing by overset method to generate computational grids of the integrated leading-edge propeller/wing configuration. QPSO algorithm was used to search for the best in the optimization design as it had high global convergence and efficiency.

2. Numerical Methods

2.1 Governing Equation

In the inertial Cartesian coordinate system, ignoring the body-force, the Navier-Stokes equation can be expressed as:

$$\frac{\partial Q}{\partial t}+\frac{\partial E}{\partial x}+\frac{\partial F}{\partial y}+\frac{\partial G}{\partial z}=\frac{NVIS}{Re}\cdot\left(\frac{\partial E_v}{\partial x}+\frac{\partial F_v}{\partial y}+\frac{\partial G_v}{\partial z}\right) \tag{1}$$

In which,

$$Q=\begin{pmatrix}\rho\\ \rho u\\ \rho v\\ \rho w\\ \rho e\end{pmatrix},\quad E=\begin{pmatrix}u\rho\\ u\rho u+p\\ u\rho v\\ u\rho w\\ u\rho h\end{pmatrix},\quad F=\begin{pmatrix}v\rho\\ v\rho u\\ v\rho v+p\\ v\rho w\\ v\rho h\end{pmatrix},\quad G=\begin{pmatrix}w\rho\\ w\rho u\\ w\rho v\\ w\rho w+p\\ w\rho h\end{pmatrix},$$

$$E_v = \begin{pmatrix} 0 \\ \tau_{xx} \\ \tau_{xy} \\ \tau_{xz} \\ kT_x + u\tau_{xx} + v\tau_{xy} + w\tau_{xz} \end{pmatrix}, \quad F_v = \begin{pmatrix} 0 \\ \tau_{yx} \\ \tau_{yy} \\ \tau_{yz} \\ kT_y + u\tau_{yx} + v\tau_{yy} + w\tau_{yz} \end{pmatrix}, \quad G_v = \begin{pmatrix} 0 \\ \tau_{zx} \\ \tau_{zy} \\ \tau_{zz} \\ kT_z + u\tau_{zx} + v\tau_{zy} + w\tau_{zz} \end{pmatrix}.$$

Equation (1) becomes Euler equation if *NVIS*=0, and Navier-Stokes equation if *NVIS*=1. ρ, u, v, w, p, e and h represent gas density, velocity component in x, y and z directions, pressure, internal energy and total enthalpy respectively.

2.2 Equivalent Actuator Disk Model

In the process of optimal design, the propeller slip flow needs to be numerically simulated for many times. In order to improve the efficiency of the flow field calculation and optimization design, the equivalent disk was used to replace the real propeller, and the acceleration and rotation effect on the airflow was simulated to obtain the slipstream effect similar to the real propeller.

Equivalent disk model simplifies the three-dimensional propeller blades rotating area to a thickness round disk. It deals with the upstream inflow and downstream outflow through the disk by the time-averaged method and the steady state approximation, so that the flow before and after the disk has the same parameters to the propeller [11,12]. The increment of airflow pressure before and after the equivalent disk generates thrust while the rotational momentum generates torque. The pressure difference and circumferential velocity difference are different at different positions of the equivalent disk.

In this paper, the front panel of equivalent disk was set as the outflow boundary and the rear panel was set as the inflow boundary, as shown in Figure 1.

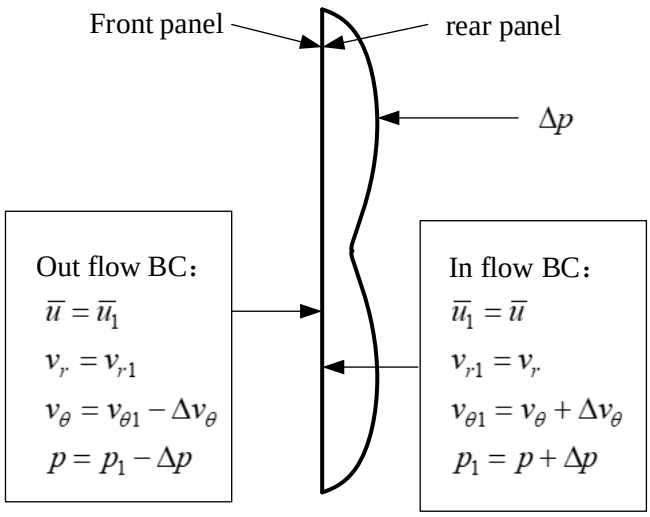

Figure 1 – Boundary condition at actuator disk.

3. Parameterization Method and Grid Deformation Method

3.1 Parameterization Method

For the propeller/wing configuration, the propeller position could be parameterized by its coordinates. FFD parameterization technique was established based on Bernstein basis functions and used for the parameterization of the wing.

The FFD algorithm could be regarded as a mapping function from physical space R^3 to mathematical space R'^3,

$$\boldsymbol{X} = F(\boldsymbol{x}) \tag{2}$$

where the input vector *x* was the logical coordinate of the entity surface to be deformed in the parameter space, and the output vector *X* was the physical space coordinate of the entity surface after deformation. Detailed procedures of FFD algorithm were referred to reference [13].

In the optimization design process, there were six design parameters in all. One was for the height of the propeller and the other five were for the airfoil of the flat wing. Figure 2 shows the FFD control frame of the wing.

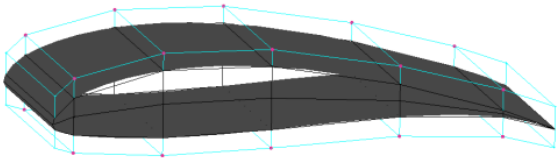

Figure 2 – FFD control frame of the wing.

3.2 Grid Deformation Method

A grid deformation method based on radial basis function interpolation was embedded in optimization for high-speed regeneration of grids around a new wing.

After obtaining the deformed surface grids by FFD method, the grid deformation technique based on the RBF interpolation was used to generate a new spatial mesh according to the original spatial mesh and boundary conditions. CPC2 type functions were employed for RBF, as they presented excellent solving adaptability and higher quality and were suitable for large deformation problems. The center point was selected from the points on the moving boundary. The corresponding scalar value was given by boundary displacements, which was specified artificially or solved by the pressure distribution of flow field and the rigid body dynamics equation of motion at the current time step.

4. Quantum-Particle Swarm Optimization Algorithm

Sun introduced the idea of quantum mechanics into particle swarm optimization (PSO) algorithm and came up with quantum-behaved particle swarm optimization (QPSO) algorithm [14,15].

Suppose *M* quantum particles were in the *N*-dimensional space. The core evolutionary equation of QPSO algorithm could be expressed as:

$$X_{i,n+1}^{j} = p_{i,n}^{j} \pm \alpha \left| X_{i,n}^{j} - C_{n}^{j} \right| \ln(1/u_{i,n+1}^{j}) \quad . \tag{3}$$

In equation (3), *X* is a particle; *i*=1,2,…,*M*; *j*=1,2,⋯,*N*; *n* is the number of currant iteration step. $p_{i,n}^{j}$ is the attractor, and

$$p_{i,n}^{j} = \varphi_{i,n}^{j} P_{i,n}^{j} + (1-\varphi_{i,n}^{j}) G_{n}^{j} \quad . \tag{4}$$

$P_{i,n}^{j}$ is the previous best (Pbest) position of particle *i*. G_{n}^{j} is the global best (Gbest) position of the particle swarm. C_{n}^{j} is the mean value of previous best (Mbest) position of all particles, and

$$C_{n}^{j} = \frac{1}{M} \sum_{i=1}^{M} P_{i,n}^{j} (1 \le j \le N) \ . \tag{5}$$

The probability of "+" is the same to "-" in "±", that is 0.5. α is an acceleration factor. $u_{i,n}^{j}$ is a random number evenly distributed in the interval (0,1), and

$$u_{i,n+1}^{j} \sim U(0,1) \tag{6}$$

5. Integrated Aerodynamic Design System

Considering slipstream effect, an integrated aerodynamic optimization design system was established based on QPSO algorithm and aforementioned methods, as shown in Figure 3. Latin hypercube sample (LHS) method was employed to select reasonable initial samples. CFD method and equivalent actuator disk Model were used to solve the slipstream flow field. QPSO algorithm was

employed to search for the optimal solution. The integrated aerodynamic design system can be extended to the design of a solar powered UAV with multiple propellers.

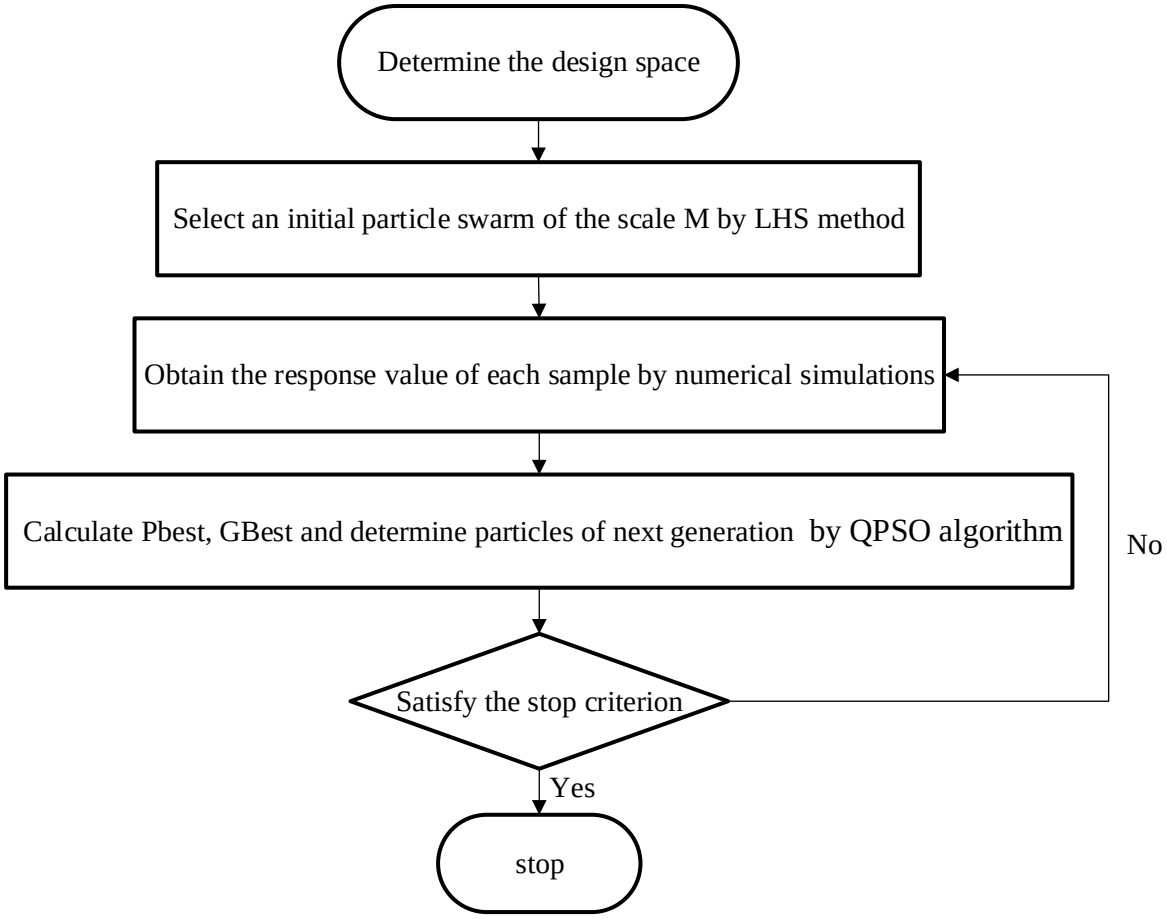

Figure 3 – Integrated aerodynamic optimization design system.

6. Results

6.1 Optimal design problem

The integrated aerodynamic design system was applied to improve the aerodynamic performance of a leading-edge propeller/wing configuration. The leading-edge configuration consisted of a section of straight wing of NACA4412 airfoil and a propeller in the front. The chord length and span length of wing were 2 m and 4 m, respectively. The propeller had two blades with a radius of 0.6 m and a revolution of 4800 rpm. The incoming flow was 20 km above the sea level at the speed of 50 m/s. The configuration was shown in Figure 4 with the computational grids. The total number of the grid cell was about 8 million.

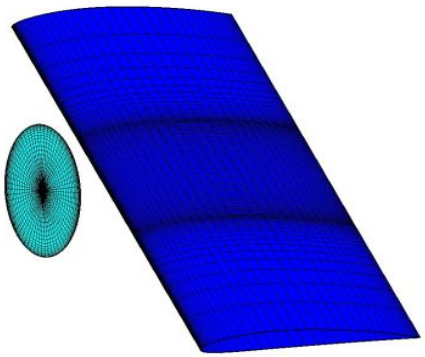

Figure 4 – Leading-edge configuration and computational grids.

Parametric modeling of the airfoil of the wing was carried out by using FFD technology with five design variables, and the range was [-0.1, 0.1]. One design variables y_p was used to describe the normal translation of propeller position, and its range was [-0.6, 0.6].

The objective of the optimization design was to improve the lift-to-drag ratio of the leading-edge configuration by optimizing the position of the propeller and the shape of the wing under the influence of slipstream in a coupled manner. The constraint conditions were that the maximum thickness of the wing should not decrease and the propeller moves along the vertical direction in a specific range. The optimal design problem could be given as follows:

$$\text{Objective function: } \min(-C_L/C_d)$$

$$s.t.\begin{cases} -0.6 \le y_p \le 0.6 \\ t_{\max} \ge 0.24 \end{cases}$$

$t_{\max}$ referred to the maximum thickness of the wing.

6.2 Results

Optimized leading-edge propeller/wing configuration was gained through the search by QPSO algorithm. Table 1 summarizes the aerodynamic characteristics of the configurations before and after optimization at cruise condition. The lift coefficient increased by 10.3% and drag coefficient decreased by 30.6%. The Friction resistance and differential pressure resistance were both significantly reduced. As a result, the lift-to-drag ratio was greatly promoted by 65.9%.

Table 1 – Aerodynamic characteristics before and after optimization.

	C_L	C_D/ counts	C_{DF}/ counts	C_{DP}/ counts	C_L/C_D
Initial	0.465	134.5	77.3	57.2	34.6
Optimized	0.513	93.3	53.2	40.1	57.4
Δ(%)	10.3	-30.6	-31.2	-29.9	65.9

As shown in Figure 5, the propeller was right in front of the wing, which meant the center of the propeller was at the same level to the leading-edge point of the wing. After the optimization search of the design system, the position of the propeller was not right in front of the wing any longer. In fact, it was shift up 0.371 m in the vertical direction.

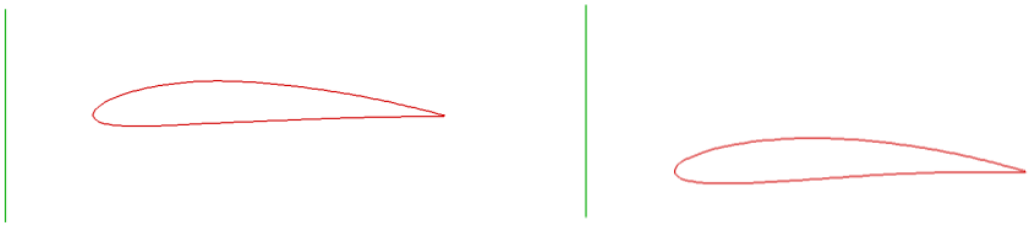

(a) Initial (b) Optimized

Figure 5 – Relative position of propeller and wing of configuration before and after optimization.

Comparing the optimized airfoil to the initial one, if we look at Figure 6, thickness of the wing hardly changed. However, the position of the maximum thickness moved forward a certain distance. For the upper surface, the profile of the leading edge becomes smoother while the profile of the trailing edge gets smoother. For the lower surface, the opposite is true.

From Figure 7, two negative pressure zones existed on the upper surface of the initial wing. It could be revealed that the leading edge of the initial wing experienced both upwash and downwash effects from propeller slipstream. These were because the initial center of the propeller was right in front of the leading edge of the wing. After design, the amounting position of the propeller was higher in the vertical direction. Therefore, the interface of two negative pressure zones was

removed, and the two zones merged into one on the upper surface of the optimized wing. The spanwise width of the negative pressure region became a little smaller, but chordwise length grew much greater.

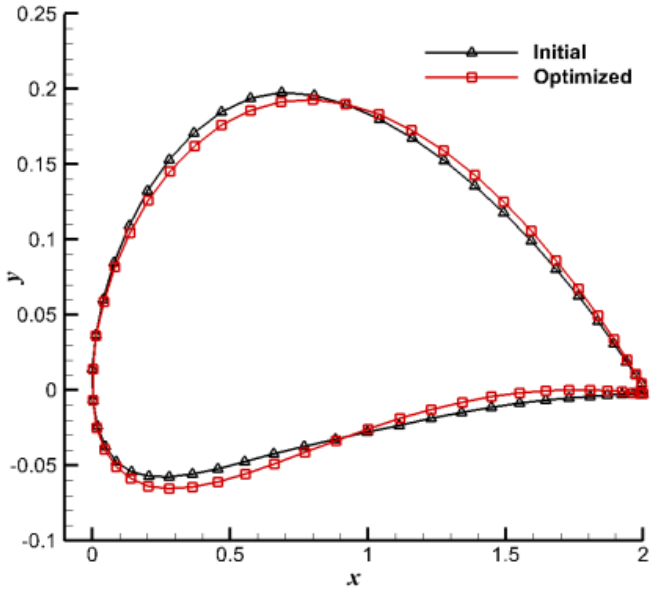

Figure 6 – Comparison of the airfoils before and after optimization.

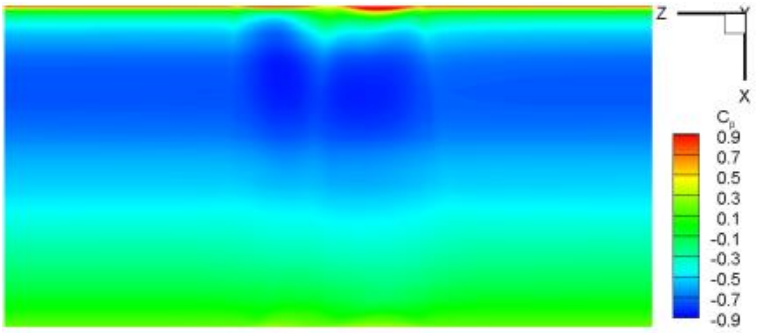

(a) Initial

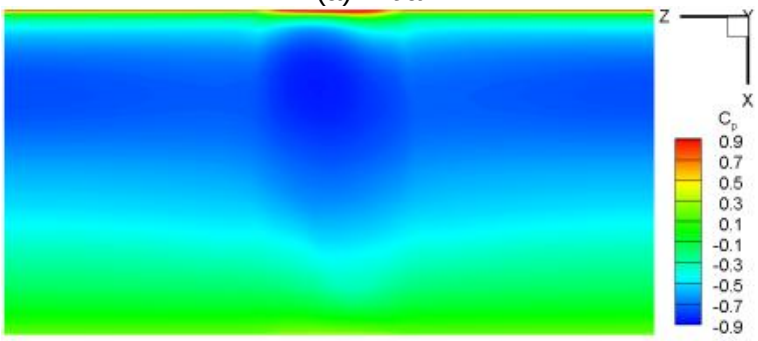

(b) Optimized

Figure 7 – Surface pressure distribution of the wings before and after optimization.

Further, the pressure coefficient distribution at different spanwise sections were compared and analyzed of the initial configuration and the optimized configuration. Figure 8 shows the comparison of pressure coefficient at the spanwise z=0.4 m before and after optimization. At this section, wings of both initial and optimized configurations were in the slipstream upwash region. Negative pressure decreased at both upper and lower surfaces after optimization, which indicated

that local upwash effect went weaker.

Figure 9 shows the comparison of pressure coefficient at the spanwise z=-0.4 m before and after optimization. Initial wing experienced downwash slipstream and intense negative angle-of –attack effect. These negative impacts got great improvement after optimization.

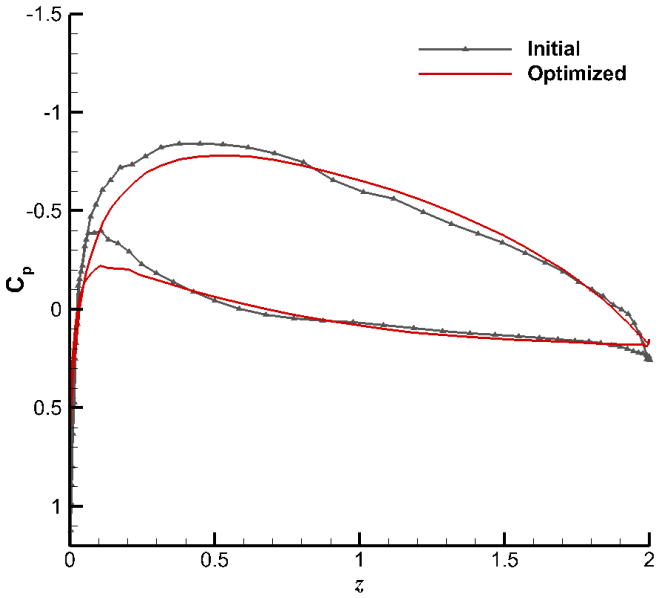

Figure 8 – Comparison of C_p at the spanwise z=0.4 m before and after optimization.

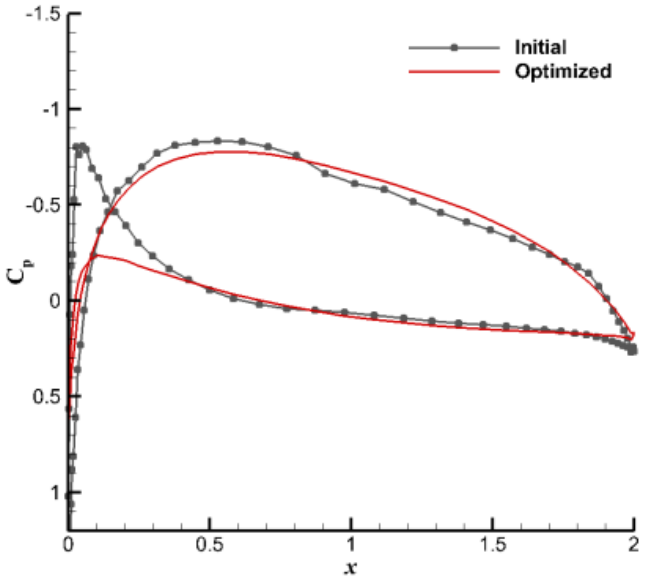

Figure 9 – Comparison of C_p at the spanwise z=-0.4 m before and after optimization.

Figure 10 shows the comparison of pressure coefficient at the spanwise z=0 before and after optimization. The optimized wing experienced much stronger upwash than the initial wing, therefore, the suction peak on the upper surface of the optimized wing grew much larger.

It could be found from Figure 8, 9 and 10 that, generally, pressure distributions at different sections along spanwise on the surfaces of the wing was much fuller and plumper after optimization. The pressure recovery on the upper surface of the wing in the slipstream areas of the propeller became more moderate and smoother. These were conducive to reducing the drag and increasing the lift of the wing.

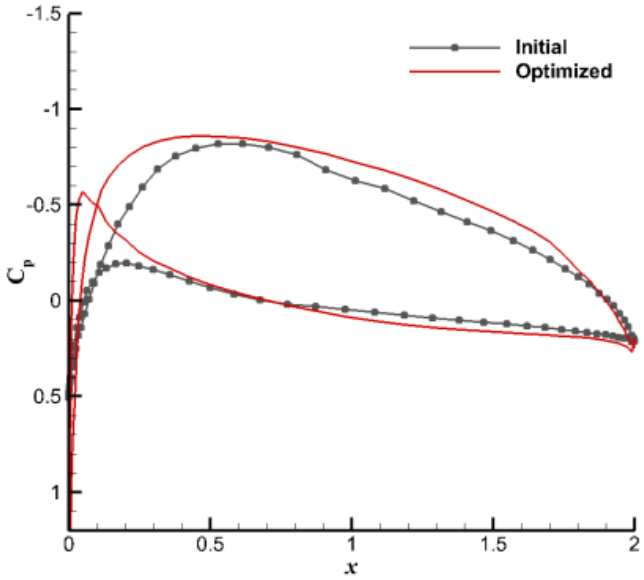

Figure 10 – Comparison of C_p at the spanwise z=0 before and after optimization.

7. Conclusions

An efficient integrated aerodynamic design system was established and applied to improve the cruise aerodynamic performance of a leading-edge configuration a low Reynolds number. It could be concluded that:

- The lift-to-drag ratio of the wing significantly increased by integrated aerodynamic optimization design to the position of the propeller and the shape of the wing in a coupled manner through the slipstream effect;
- The integrated aerodynamic design method could be extended to high altitude and long endurance solar powered UAVs with multiple propellers for heavier mission load and lower energy consumption by improving their integrated aerodynamic performances.

As a future work, the present design method will be applied for complex geometries with multiple-propeller configuration.

8. Contact Author Email Address

The contact author email address: yangwei_cardc@sina.com.

9. Copyright Statement

References

[1] Romeo, G and Fulla, G. Aerodynamic and structural analysis of HAVE solar platform. *AIAA 1st Technical Conference and Workshop on Unmanned Aerospace Vehicles*. Reston, VA: AIAA, 2002.

[2] Wang Y K. Application prospect and development analysis of near space vehicle. *National defense science and technology*. Vol. 30 No.2, pp 20-24, 2009. (in Chinese)

[3] Wang Y F, An Y W and Yang J H. Current status and development trend of near space vehicles. *Fundamentals of National Defense Technology*. Vol. 1, pp 33-37, 2010. (in Chinese)

[4] Rakshith B R, Deshpande S M, Roaddam N, et al. Optimal low-drag wing platforms for tractor-configuration propeller-driven aircraft. *Journal of Aircraft*. Vol. 52 No.6, pp1-11, 2015.

[5] Wang K L, Zhou Z, Zhou X P. Aerodynamic design of low Reynolds number wing coupled with multiple propellers induced effects. *Acta Aeronautica et Astronautica Sinica*. Vol. No.6, 120813, 2017. (in Chinese)

[6] Moore M and Fredericks B. Misconceptions of electric propulsion aircraft and their emergent aviation markets. *52nd Aerospace Sciences Meeting*. National Harbor, MD, AIAA 2014-0535, 2014.

[7] Xu D K. NASA restructures aeronautic research programs. *International Aviation*. Vol. 3, pp 69-71, 2015. (in Chinese)

[8] Gohardani A S, Doulgeris G D and Singh R. Challenges of future aircraft propulsion: A review of distributed propulsion technology and its potential application for the all-electric commercial aircraft. *Prgress in Aerospace Sciences*. Vol.47, pp 369-391, 2011.

[9] Patterson M D, Daskilewicz M J and German B J. Distributed propellers: multidisciplinary analysis needs and aerodynamic modeling development. *52nd Aerospace Sciences Meeting*. National Harbor, MD, AIAA2014-0534, 2014.

[10] Wang K L, Zhu X P, Zhou Z, et al. Distributed electric propulsion slipstream aerodynamic affects at low Reynolds number. *Acta Aeronautica et Astronautica Sinica.* Vol. 37, No.9, pp 2669-2678, 2016. (in Chinese)

[11] Strash D J, Lednicer D A and Rubin T D. Analysis of propeller-induced aerodynamic effects. AIAA 98-2414, 1998.

[12] Li B, Liang D W, Huang G P. Propeller slipstream effects on aerodynamic performance of turbo-prop airplane based on equivalent actuator disk model. *Acta Aeronautica et Astronautica Sinica*.Vol. 29, No.4, pp 845-852, 2008. (in Chinese)

[13] Xu J K, Bai J Q ,Huang J T, et al. Aerodynamic optimization design of a wing under the influence of slipstream effect. *Acta Aeronautica ET Astronautica Sinica*. Vol. 35, No. 11, pp 2910-2920, 2014.

[14] Sun J, Fengand B and Xu W. A global search strategy of quantum-behaved particle swarm optimization. *Proc.2004 IEEE Conference on Cybernetics and Intelligent Systems.* Singapore, pp 111-115, 2004.

[15] Sun J, Fang W, Palade V, et al. Quantum-behaved particle swarm optimization: analysis of individual particle behavior and parameter selection. *Evolutionary Computation*. Vol. 20, No.3, pp 349–393, 2012.